Article

Physical, Thermal, and Chemical Properties of Fly Ash Cenospheres Obtained for Different Sources

Andrei Shishkin*[1], Vitaliijs Abramovskis[1], Ilmars Zalite[2], Ashish Kumar Singh[1], Gundars Mezinskis[2], Vladimir Popov[3] and, Jurijs Ozolins[1]

[1] Rudolfs Cimdins Riga Biomaterials Innovations and Development Centre of RTU, Institute of General Chemical Engineering, Faculty of Materials Science and Applied Chemistry, Riga Technical University, Pulka 3, K-3, Riga, LV-1007, Latvia; andrejs.siskins@rtu.lv (A.S.), vitalijs.abramovskis@edu.rtu.lv (V.A.), aksingh@nyu.edu (A.K.S.), Jurijs.Ozolins@rtu.lv (J.O.)

[2] Institute of Materials and Surface Technologies of the Riga Technical University, P. Valdena iela 7, Riga, LV-1048, Latvia; ilmars.zalite@rtu.lv (I.Z), gundars.mezinskis@rtu.lv (G.M.

[3] Department of Materials and Engineering, Tel Aviv University, Tel Aviv 6997801, Israel. vpopov@tauex.tau.ac.il

* Correspondence: andrejs.siskins@rtu.lv

Abstract: Cenospheres are hollow particles in fly-ash, a by-product of coal burning, and are widely used as reinforcement for developing low density composites called syntactic foams. This study investigates the physical, chemical, and thermal properties of cenospheres obtained from 3 different sources, CS1, CS2, and CS3, for the development of syntactic foams. Description of floatation method to separate broken particles is given, and it was seen that up to 11 % of the particles were damaged. Post heat treatment samples show development of SiO_2 phase in the cenosphere, which is not present in the as received product. CS3 had the highest quantity of Si element, compared to the other two, showing the difference in the source quality. The particle size distribution for CS2 is very narrow while for the others is much broader. All censopheres have porous walls but the morphology of CS2 is the most uniform and smooth. For the application of metallic layer and subsequent consolidation via spark plasma sintering, CS2 was deemed the most physically, thermally, and chemically suitable.

Keywords: Hollow microballons; cenospheres; ceramics phase composition; chemical composition

1. Introduction

In recent years, syntactic foam (SF) composites have increasingly found use in various industries where superior mechanical strength at a low weight is desired. The SF made of polymer or metal in between hollow microspheres [1–3]. Syntactic foam with specific properties can be obtained by reinforcing hollow particles in a polymer, metallic, or ceramic matrix. Syntactic foams are increasingly being used by excellent mechanical strength and stiffness-to-weight ratios [4,5] Such materials are used in aviation, space technology, and ship construction to manufacture individual parts [6,7].

A promising material for obtaining syntactic foam is cenospheres (CS), hollow alumosilicates hollow micro balloons. CS is produced as a waste product when burning in thermal power plants (TPC) in the composition of light ash of coal, as a result of complex thermochemical processes [8]. Recently, coal thermal power plants have produced about 41% of global electricity, which is expected to increase to about 44% by 2030 [8]. This combustion of coal results in the production of large quantities of waste called fly ash. It is estimated that approximately 750 million tonnes of fly ash are produced annually worldwide, and the rate is increasing at a high rate. A large quantity of fly ash is disposed of in landfills and ash lagoons. Due to the heavy metal leaching and high cost of landfills, many

Preprints (www.preprints.org) | NOT PEER-REVIEWED | Posted: 5 January 2023 doi:10.20944/preprints202301.0090.v1

applications have been suggested to convert this waste into value-added products. To increase the re-use of coal fly ash, several separation methods have been developed to segregate value-added components, such as aluminosilicates, magnetite, and CS from solid particles and unburned carbon [8]. CS can be separated from the ashes by the method of flotation; in the lagoons, they float to the surface of the water, from where they can be collected for further processing. The CS world market is up to 600 million dollars annually, equivalent to 700 – 800 tons [9,10]. The main suppliers of CS in the world are China, India, Russia, Kazakhstan, and Ukraine. As a waste product of TPC operations, CS are available at a relatively low cost.

Cenospheres account for an average of 0,01 to 4,80 % by mass of fly ash. They are characterised by low bulk density (0.4-0.72 $g \cdot cm^{-3}$), very low thermal conductivity (about 0.065 $W \cdot m^{-1} \cdot K^{-1}$) and excellent stability in alkaline solution and to high temperatures. The particle size of the CS ranges from about 5 to 500 μm [8,11]. By chemical composition, these materials belong to multi-component systems with a SiO_2–Al_2O_3–Fe_2O_3 content of approximately 90 wt% [12–14]. The utilisation of fly ash is determined by ◎ts properties, such as fineness, specific surface area, particle shape, hardness and freeze-thaw resistance, [15,16].

The properties of microspheres and significant accumulations can be recycled long-term and used to create new functional materials with high added value. CS is very widely used in the manufacture of stuffed building materials with reduced density and improved thermal insulation properties [9,10], CS is also used as filler and reinforcement in metal-matrix composites [17–19] ceramics-matrix composites [20–22], polymer-matrix composites [23,24] and various hybrid matrix composites [21,25].

A promising direction of their use may be to manufacture lightweight and mechanically resistant multi-layered composite materials with specific properties. Previous work show a proof-of-the-concept of the obtaining of the novel (matrix-less) SF [26,27] obtained by using CS from burning coal from the Donetsk and Ekibastuz coal basins TPC. As described in works [26,27] matrix-less SFs were obtained by spark plasma sintering (SPS) of metallised CS (Me@CS) at the temperature range from 800 ° (for Cu) and up to 1150 °C in the case of Ti and 316 steel coating. Micron and a sub-micron layer of metal (Cu, Ti and 316 steel) [26,27] were deposited by physical vapour deposition (PVD).

The development of SF from metallised CS has been studied previously and by other researchers as well. However, the effect of the heat-treatment and processing on the properties of CS, as well as the difference between the behaviour of CS obtained from different sources is not well understood. It is especially important to understand this given the prevailing geopolitical situation, which makes it challenging to the source of raw materials with the same ease and availability. Since the properties of CS depend on the type of coal and the conditions for its TPC, CS has a wide range of properties [8,11]. The purpose of this work is to understand the quality of raw material, the effect of heat treatment on the CS, and its characterisation, which could be suitable for novel matrix-less SF precursor preparation. In this research, the phase change that occurs in the CS during the pre-treatment will be studied. The physical and chemical properties of raw CS and metallised CS are studied to better inform and guide subsequent processes, i.e., the development of SF and its mechanical properties.

2. Materials and methods

The cenospheres used in the current study were a by-product of coal-fired plants from the Donetsk and Ekibastouz coal basins, burning them in various TPC. The origin, designation and particle size characteristics of CS are shown in Table 1.

Table 1. Source designation and granulometric composition of CS.

Preprints (www.preprints.org) | NOT PEER-REVIEWED | Posted: 5 January 2023 doi:10.20944/preprints202301.0090.v1

Sample designation	Coal field	Grading composition* (μm)
CS1	Donetsk	40 - 500
CS2	Donetsk	40 - 200
CS3	Ekibastuz	50 - 300

*- according to the supplier data

Determination of particle size distribution (PSD) was carried out with the help of the vibratory sieve shaker Analysette 3 PRO (FRITSCH GmbH Idar-Oberstein, Germany). Particles were fractioned using sieves with opening sizes of 0.05, 0.10, 0.15, 0.20, 0.25 and 0.30 mm. The bulk density was determined by using a bulk density tester (Scott volumeter, according to ASTM B 329-98, Copley, Nottingham, UK). For obtaining the true particle density (TPD), a Quantachrome Ultrapyc 1200e (Anton Paar GmbH, Graz, Austria) automatic gas pycnometer was used.

Specific thermal conductivity was determined by LaserComp (ASV) Fox 600 measuring equipment, the sample was freely poured in a layer with a thickness of 30 mm.

2.1. Determination of the interparticle voids fraction

Before producing syntactic foams, it is essential to know the maximum achievable packing density or its opposite value – interparticle voids fraction ε. This value gives the maximum volume fraction (VF) of CF that can be dispersed in the matrix. The maximum possible packing density for spherical particles is known to be 0.741 [28,29]. In the case of practically monodisperse particles, with possible dense packing (random close packing), this value can reach 0.64 [30,31], in the case of real loose packing (random loose packing), it usually does not exceed 0.60 [30]. This means that an actual interparticle voids fraction is not less than ε = 1–0.60 = 0.4. The determination of interparticle void or volume filling coefficient ε, was calculated using Eq (1)

$$\varepsilon = \frac{V-(V_{p+fl}-V_{fl})}{V} \quad (1)$$

Where:

V – the volume of the particles in bulk condition, prepared by with Scott volumeter,

V_{p+fl} – the volume of the mixture (particles + fluid),

V_{fl} – the volume of the fluid

A method for determining the CS interparticle voids was developed. The essence of this is as follows. The volume of the particles in bulk condition (V) is the sum of the volume occupied by the particles and the interparticle voids volume, which can be determined by filling the voids with a certain volume of fluid V_{fl}. Since the bulk density of CS is usually in the range of 0.38 to 0.43 g·cm^{-3}, it is impossible to perform the experiment using water correctly. The forces acting on a dispersed particle in a viscous medium are described by Stokes's law, which states that the sedimentation rate of a particle under other independent conditions is proportional to the difference between the densities of the particle and the medium and inversely proportional to the viscosity of the medium. The kinetic persistence of dispersed systems (or, more simply, the sedimentation speed of particles or particle's rise speed) is described by Stokes's law, Eq (2)

$$V_S = \frac{d^2 g(\rho_p-\rho_{fl})}{18\,\mu} \quad (2)$$

where V_S - sedimentation speed of particles (m/s) (if$\rho_p > \rho_{fl}$) or particles rise speed to the surface of a liquid (if$\rho_p < \rho_{fl}$).

d – diameter of the particle (m),

g – acceleration of gravity (m·s^{-2}),

 doi:10.20944/preprints202301.0090.v1

ρ_p – single particle apparent density (kg·m^{-3}),

ρ_{fl} – density of the fluid (kg·m^{-3}),

μ - dynamic viscosity of the fluid (Pa·s).

Based on Stokes's formula (2), sedimentation (stratification) speed is directly proportional to the particle diameter, the phase difference, and the square of the density of the environment, as well as inversely proportional to the viscosity of the environment. Therefore, to reduce the sedimentation rate, e.g., increase resistance to sedimentation, different methods can be used, such as increasing the viscosity of the environment using disperses with a density close to the density of the substance.

The simplest way is increasing the viscosity of the environment dispersion. To control the viscosity solution of potato starch in distilled water (10 g·l^{-1}) with 0.01% (−)-Ethyl L-lactate (purists. p.a., cleaning grade, ≥98.0% (sum of enantiomers, GC), supplier - Fluka (now Sigma-Aldrich) as surfactant, was used. The exact volume of CS (25 cm^3) under investigation was obtained with Labulk-0302 Scott Volumeter (Version ISO 3923-2) to ensure actual bulk density, and then 25 cm^3 of CS was mixed with a precise (100.0 cm^3) volume of starch solution, the system was degassed, and precise volume measurement was taken.

2.2. *Determination of the ratio between intact and defective cenospheres*

To obtain the highest quality syntactic foam from metallised CS, separating the intact CS from damaged ones is necessary. The damaged CS can be: broken, porous and/or cracked from handling or processing. For this, the flotation method was chosen, implemented as follows. A solution consisting of 800 cm^3 of distilled water and 50 cm^3 of ethanol (to reduce surface tension) was prepared, and 100 g of CA was added and stirred with a glass rod for 60 seconds. The mixture was sifted for 5 minutes, then the floating fraction (with the aid of a spatula and decantation) was carried to the next beaker with fresh washing liquid, and the procedure was repeated. After repeated settling of the upper layer, it was transferred to a Buchner funnel and washed with ethanol. Then it was dried in an oven at 105 °C for 12 hours with a layer of no more than 20 mm. To determine the ratio of intact and destroyed CAs, Liquid below settlings was being decanted carefully; sediments were carried to the Büchner funnel; rinsed with distilled water, and then by ethanol; dried in an oven at 105°C for 12 hours.

2.3. *Morphology, chemical and phase composition*

A Scanning Electron Microscope (SEM) Zeiss EVO MA-15 EDS equipped with INCA Energy 350 was used to evaluate CS morphology and element composition. For the element composition. For the phase composition determination, powder X-ray diffraction (XRD) on the diffractometer BRUKER D8 Advance with Cu anode, accelerating voltage 40 kV and beam current 40 mA. For quantitative analysis, the Rietveld method with internal standard mineral corundum was used.

High-temperature optical microscope (EM201 HT163, Hesse instruments, Germany) was used for 2D-dilatometry. 2D-dilatometry is an optical dilatometry – cross-section measurements of the specimen's area. The heating mode was set as follows: up to 800 °C, the heating rate was 20 °C·min^{-1}, since up to this temperature the deformations of the CS are unlikely to occur but heating above 800 °C was carried out at a speed of 5 °C·min^{-1}.

Fourier transform infrared (FTIR) spectra were recorded using Thermo Scientific Nicolet™ iSTM50 (Thermo Fisher) spectrometer in the Attenuated Total Reflectance (ATR) mode. Spectra were obtained over a range of wavenumbers from 400 cm^{-1} to 4000 cm^{-1} co-adding 64 scans at 4 cm^{-1} resolution. Before every measurement, a background spectrum

Preprints (www.preprints.org) | NOT PEER-REVIEWED | Posted: 5 January 2023 doi:10.20944/preprints202301.0090.v1

was taken and deducted from the sample spectrum.

2.4. *Material preparation and study*

It is necessary to understand the thermal-structural relationship for CS in order to obtain advanced SF, since the method of foam synthesis if SPS. Sintering of metallised CS takes involves the melting and fusion of metal coating that can reach temperatures in the range of 1100 – 1200 °C [32]. The composition of CS are refractory ceramics that can withstand the high temperatures, but it is necessary to investigate the effects of this thermal treatment on the CS.

The process flowchart for the study is shown in Figure 1, which describes the treatment and characterization steps taken for cenospheres CS1, CS2 and CS3. The bulk density (ϱ_{bk}), pycnometric density(ϱ_{py}), interparticle voids fraction (ε), PSD, SEM, phase composition and 2D-dilatometry (HTM analysis). To assure high quality of metal-CS foam by sintering of metallised CS, is necessary to separate the intact CS from the damaged. For this purpose, the flotation method is used with liquid media – water. After the separation of damaged CS (broken, porous and cracked) and unburned coal particles was studied 1100 and 1200 °C thermal treatment influence on the CS.

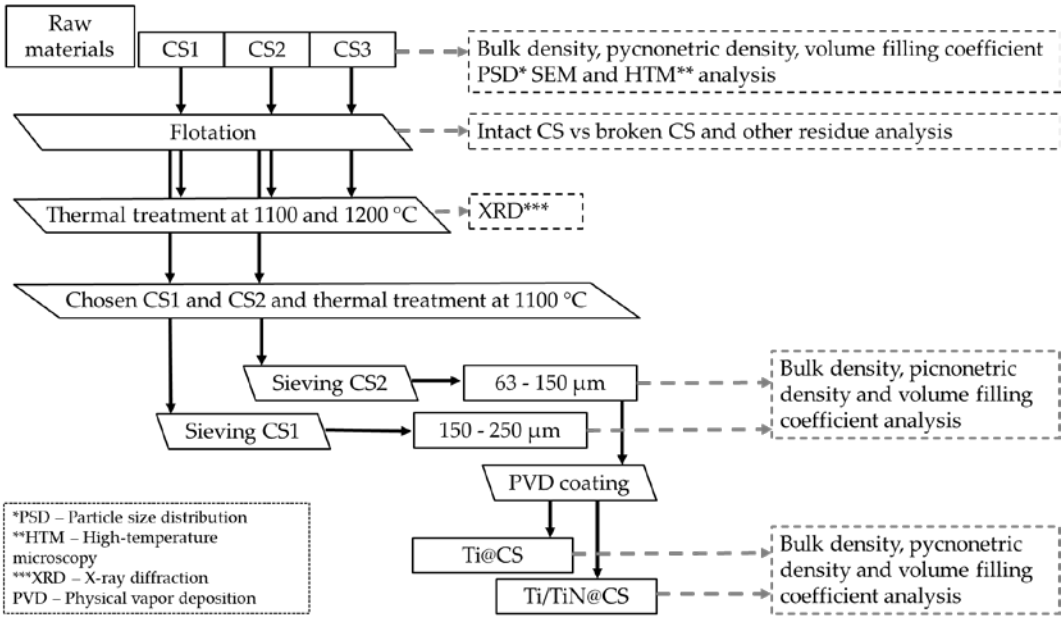

Figure 1. Flowchart depicted the process flow and characterization after each step.

3. Results

3.1. *Granulometry composition, the density of CS*

For all types of CS, the PSD was obtained. As can be seen from Figure 1., the CS used in experiments are predominantly (more than 40%) in the 100 to 150 μm size range. In the case of CS1, up to 14% are particles < 100 μm, and about 27% are particles >150 μm. In the case of CS2, particles with average sizes of 100 - 150 μm are mainly present, while in CS3, particles (up to 42%) with sizes of 100 - 150 μm and particles > 200 μm (up to 15%) are observed. From a granulometric point of view, a more even distribution of CS particles is in the case of CS2: above 74% with dimensions from 100 to 150 μm.

Preprints (www.preprints.org) | NOT PEER-REVIEWED | Posted: 5 January 2023 doi:10.20944/preprints202301.0090.v1

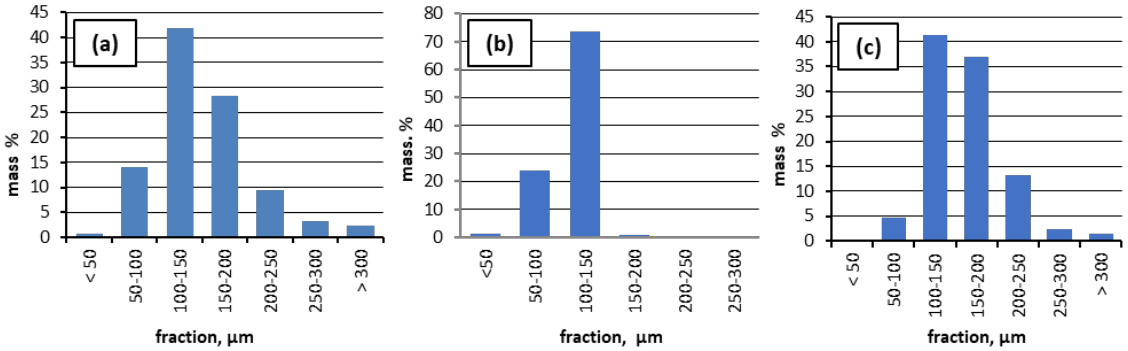

Figure 2. Particle size distribution (PSD) of the three types of cenospheres (a) CS1, (b) CS2, and (c) CS3.

An important indicator is the bulk density of the material, the interparticle voids fracrion, as well as the density of the material of the globular wall. Experimental data are summarised in **Table 2**. The lowest bulk density is observed in the case of CS2, which may be due to a more even particle size distribution, as was seen in Figure 1. Dispersions with different particle sizes during the pouring are arranged more densely, which leads to an increase in bulk density and a decrease in the interparticle voids volume. The pycnometric density after heat treatment at 1100 °C increased from 2.153 to 2.178 g·cm^{-3} in the case of CS1 raw material. In case of CS1 pycnometric density mainly correspond to CS wall material – ceramics and could have density change due to phase composition change. In the case of CS2 pycnometric density decreased from 2.272 to 2.185 g·cm^{-3}. This fact could be explained by the burning out of residual coal particles (LOI=0.4) during the thermal treatment (**Table 4, Figure 9**), and the significant amount of broken CS (11.6%) content in the CS2 sample, which is separated later by flotation method for preparing the CS 63-150 µm fraction. Ti and Ti-TiN coated CS has greater pycnometric density, which is obvious, due to deposited Ti and Ti-TiN.

Table 2. Bulk density of CS, the density of the material and interparticle voids fraction.

Material	Bulk density, g·cm^{-3}	Pycnometric density g·cm^{-3}	Interparticle voids, %
Raw CS1	0.415±0.004	2.153±0.001	40.0
Raw CS2	0.380±0.002	2.272±0.001	43.0
Raw CS3	0.411±0.004	2.301±0.001	38.0
1100 ° treated CS 63-150 µm	0.39±0.004	2.185±0.001	44.0
1100 ° treated CS 150-250 µm	0.41±0.004	2.178±0.001	46.0
1100 ° treated CS 63-150 µm Ti@CS	0.40±0.004	2.661±0.001	44.0
1100 ° treated CS 63-150 µm Ti-TiN@CS	0.42±0.004	2.531±0.001	43.0

3.1. Chemical composition

In order to more fully characterise the microspheres studied, it is important to find out and compare their chemical composition, which can differ significantly when burning different coals at different temperatures. Energy dispersive X-ray spectrometry (EDS) data from the surface of raw microspheres show that the main elements present in their shell are Al, Si, Fe, Ca, Mg, K, Na, O, and in significant quantities C. Average composition of microsphere material elements from EDS analysis data is shown in Table 3.

Preprints (www.preprints.org) | NOT PEER-REVIEWED | Posted: 5 January 2023 doi:10.20944/preprints202301.0090.v1

Table 3. Average CS, CS2 and CS3 element analysis in at. %.

Sample	C	O	Al	Si	Fe	Ca	Ti	Na	K	Mg	Si/Al*
CS1	10.04	55.48	14.92	17.37	0.31	0.25	0.29	0.23	-	0.02	1.16
CS2	8.94	57.16	15.25	16.76	0.24	0.04	0.33	-	-	-	1.10
CS3	11.49	53.00	8.50	21.00	2.02	0.05	0.40	-	2.0	0.74	2.47

Si/Al* - Si/Al at. ratio

It should be noted that the composition of the material is sufficiently uneven for all samples. In the case of, samples CS1 and CS2 have the same elemental composition and Si/Al ratio, then sample CS3 is significantly different. The content of the element Al has practically been reduced twice, Fe and K appear in the composition of the material in noticeable quantities. For all samples, elemental analysis shows significant amounts of carbon, which could be explained by carbon not fully burned.

The studied samples were thermally treated at a temperature of 1000 °C and chemical analysis was performed, the analysed elements were converted to oxides (see Table 4).

Table 4. Chemical composition of cenospheres

Sample	SiO_2	Al_2O_3	Fe_2O_3	CaO	MgO	Na_2O	K_2O	LOI* 400 °C,%	LOI*1000 °C,%
CS1	56,5	36,9	1,4	2,4	1,2	1,1	0,5	0,5	0,1
CS2	53,8	40,7	1.0	1,4	0,6	0,5	0,4	0,6	0,4
CS3	61,4	24,4	3.4	1,9	1,6	0,5	2,2	3.9	0,2

* LOI – Lost of ignition.

The results of the chemical analysis confirm the obtained EDS data - CS1 and CS2 are close enough in composition, but CS3 is significantly different. Also, the main differences are in the proportions of SiO_2 and Al_2O_3 and in the content of Fe_2O_3. It should also be mentioned that the mass loss during heating in the case of sample CS3 is on average 7 times higher than in the other samples.

3.2. The ratio between intact and defective cenospheres

When analysing the CS samples CS1, CS2, and CS3, it was found that after settling (segregation in floating and non-floating fractions) samples CS2 and CS3 (**Figure 3**), the liquid turned black. After filtering, black deposits remained on the filter. Sediment analysis was not carried out, but it is believed to have been formed by particles of coal that had not burned out. In the sample, the CS1 liquid became gray-yellowish.

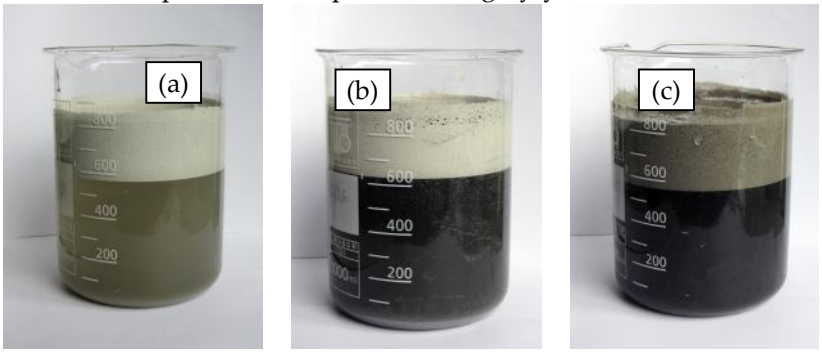

Figure 3. Images of beakers with water and CS1 (a), CS2 (b), and CS3 (c) showing the setup used for separating the broken and intact particles.

Preprints (www.preprints.org) | NOT PEER-REVIEWED | Posted: 5 January 2023 doi:10.20944/preprints202301.0090.v1

Results of floating and non-floating microsphere fractions, as well as calculation of percentage of fraction are: 1.1±0.05% defected microspheres in sample CS1, in CS2 - 11.6±0.09%, in CS3 - 3.2±0.08%. In the contents of samples CS2 and CS3, possibly, coal particles not burned out were present.

3.3. *Determination of crystalline phases in cenosphere composition*

To determine phase composition of the CS and how it is affected by heat treatment, X-ray diffraction (XRD) phase analysis was performed on as received and heat treated CS. The heat treatment of the CS was performed at 1100 and 1200 °C in accordance with the process flow shown in **Figure 1**. Cenospheres form a small fraction of the fly-ash that is produced as a by-product of mineral component of coal when they burn at high temperatures, with the formation of crystallite mixtures and a glass phase. The diffractograms for the CS1 CS2 and CS3 are shown in **Figure 4**. As shown by X-ray studies, the diffractograms of samples CS1 and CS2 are very lax. In the output samples, the mullite $Al_6Si_2O_{13}$ and the amorphous phase, which can be attributed to the glass phase, can be observed mainly. Mullite is the main crystalline phase, which occurs as a result of thermochemical transformations of alumino–silicates contained in coal. When the samples are heated at 1100 °C and 1200 °C, the phase of cristobalite SiO_2 is shown, and its intensity increases with increasing heat treatment temperature (sample diffractograms are shown in **Figure 4**). The cristobalite (SiO_2) phase is not seen in the as-received samples from all sources, but upon heat treatment, it is seen that the amount of cristobalite phase increases, showing that heat treatment leads to the formation of cristobalite. Along with that, the net amount of mullite phase also increases, indicated by the increase in peak height.

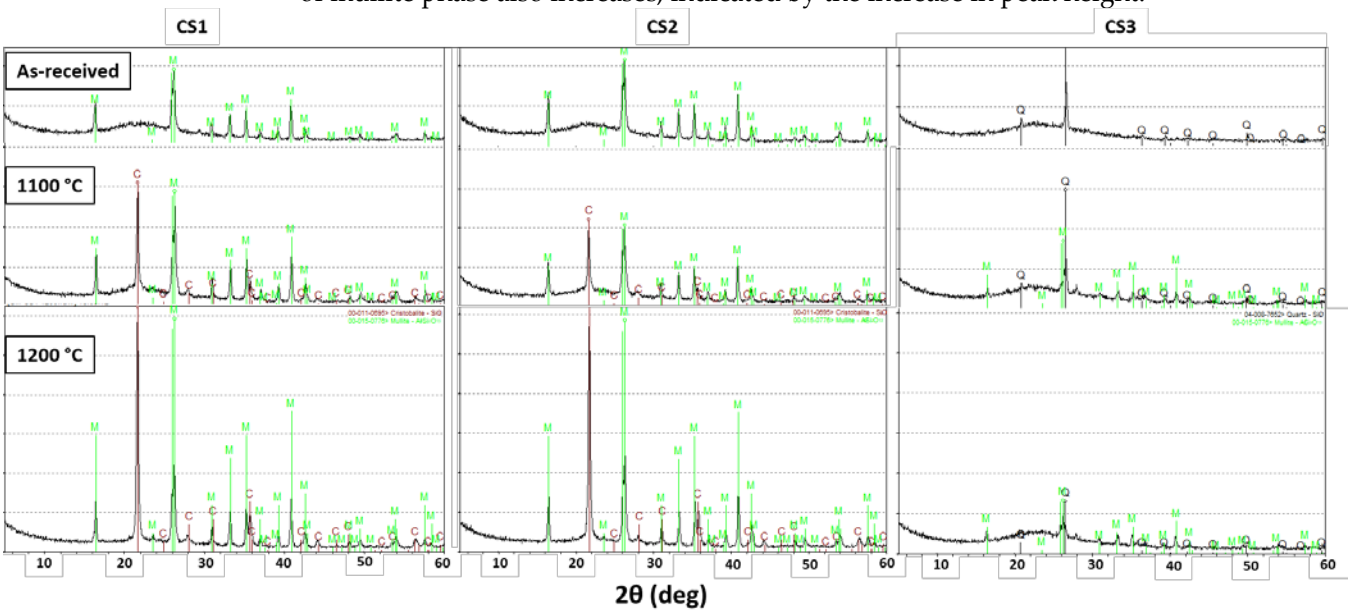

Figure 4. X-ray diffractograms of the CS at as received and heat-treated conditions. Phase designations: C/Q – Cristobalite SiO_2; M – mullite $Al_6Si_2O_{13}$.

Sample CS3 differs from the rest in terms of phase composition, showing that it is less crystalline than CS1 and CS2. Also, SiO_2 is already present in polymorphic modification of quartz in the untreated sample, and mullite forms as after heat processing. Moreover, in sample S3, the amount of amorphous phase after heat treatment is much higher than the other two samples (the characteristic plateau on the X-ray diffraction pattern is indicative of this), but in samples CS1 and CS2 it turned into crystalline phase.

Preprints (www.preprints.org) | NOT PEER-REVIEWED | Posted: 5 January 2023 doi:10.20944/preprints202301.0090.v1

Sharply different are the diffractograms of the sample CS3. In the output sample, only the crystalline phase of quartz at 26.2 degrees at 2θ and the X-ray phase are detected with a decrease in the concentration of Al_2O_3, that is, with an increase in the ratio SiO_2/Al_2O_3, the quartz phase prevails. The heat treatment of the samples causes the quartz phase to decrease and the formation of the mullite phase.

Figure 5 shows the visible FT-IR spectra of the microspheres studied show a wide absorption band in the interval of 1058 – 1062 cm^{-1}, which can be attributed to the valence and deformation oscillations of Si-O-Si(Al) in the crystal lattice and v=820 cm^{-1} to valence oscillations in the case of Si-O CS1 and CS2. In the case of CS3, a pronounced band at 1008 cm^{-1} appears, which is attributed to valence oscillations in the bridge links in the Si-O-Si(Al) crystal lattice. A small maximum also indicates the presence of quartz in the case of CS3 at 778 cm^{-1} [33]

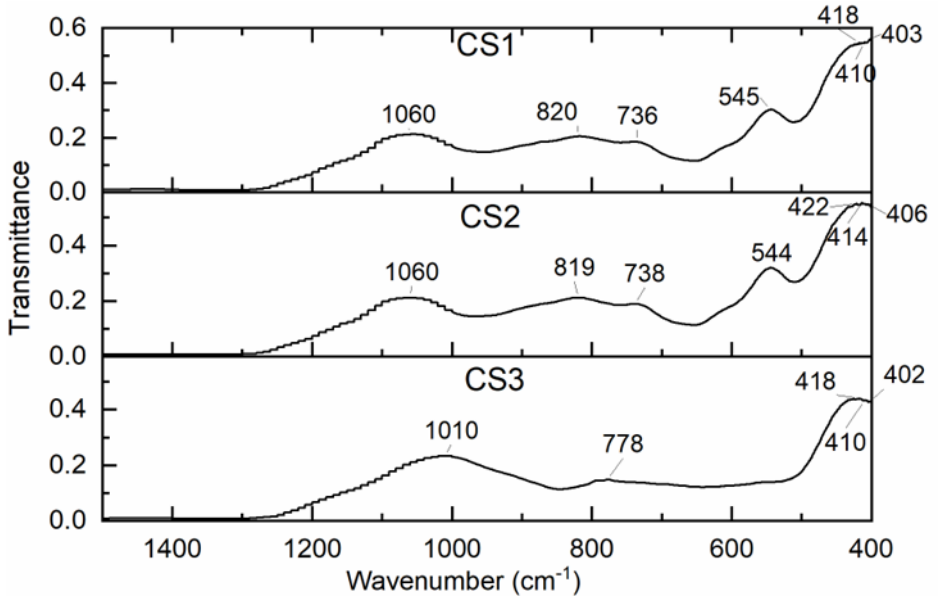

Figure 5. The FT-IR spectra of the cenospheres CS1, CS2, and CS3.

At various types of oscillations, Si-O-Al, Al-O, Si-OH, and Si-O can be attributed absorption bands in the interval of 800 – 420 cm^{-1}. The position of the absorption bands and their intensity in the IR spectra are significantly influenced by the ratio in the structure of Si/Al microspheres. Moreover, this is not about pure materials, but about a technical product with a sufficiently heterogeneous composition.

3.4. The morphology of the CS

The chemical and phase composition of CS largely determines the morphology of their surface. Figure 3. microphotographs of cenospheres SEM can be seen, in which three different types of individual microspheres of the surface can be distinguished.

Cenospheres in sample CS1 (**Figure 6**a) can be seen having different globular sizes, most of the surface is embossed and perforated. In the case of CS2 (**Figure 6**b), the particles are of uniform size and predominantly globular shape with smooth surface. CS3 microspheres (**Figure 6**c) have a wide variety of morphological forms and a significant part of the weight are damaged. The walls of the particles have distinct porosity. The variety of shapes and surface conditions of CS is explained by the very complex processes of transformation of oxide formation and crystallisation after coal burning during separate stages of their combustion at high temperatures.

Preprints (www.preprints.org) | NOT PEER-REVIEWED | Posted: 5 January 2023 doi:10.20944/preprints202301.0090.v1

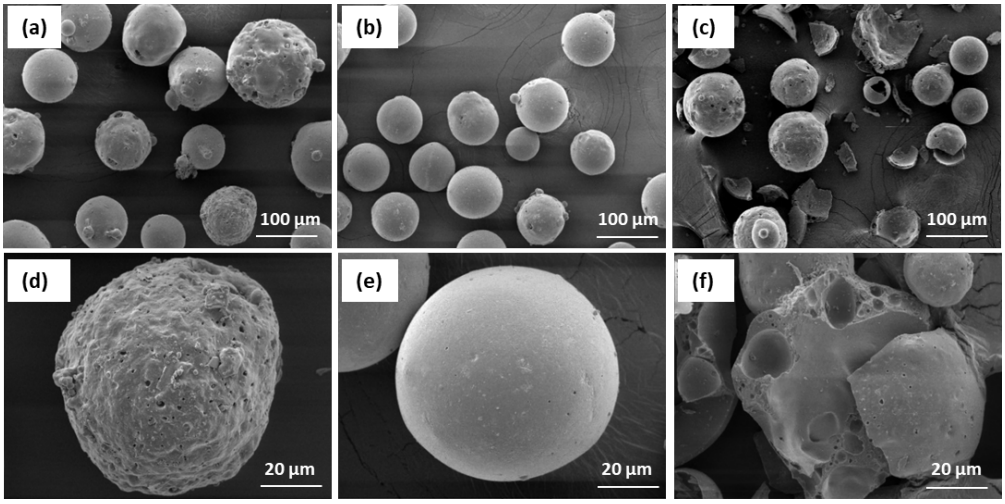

Figure 6. SEM micrographs of the cenospheres.

In order to be able to judge the thickness of the wall of the shapes of the CS shells and its structure, resin-fixed CS grindings were made (**Figure 7**). In most cases, when the CS have a pronounced spherical shape, the shell wall thickness is from 4 to 10 µm on average. As can be seen, the walls have close porosity with average pore sizes is from 0.5 to 5.0 µm. Also, it is clearly seen that CS3 has greater wall close porosity among all studied CS.

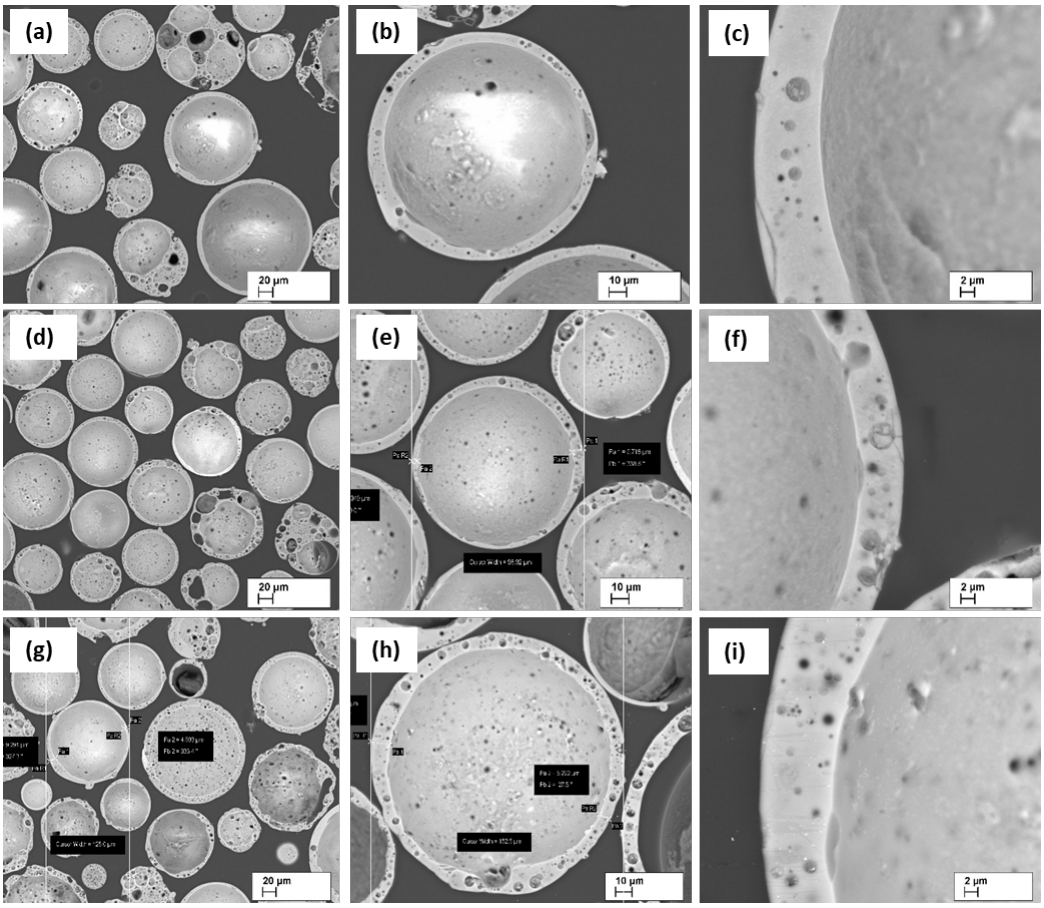

Figure 7. SEM micrographs of CS1 (a-c), CS2 (d-f), and CS3 (g-i) at 200, 500, and 2000 × times magnifications, respectively.

Preprints (www.preprints.org) | NOT PEER-REVIEWED | Posted: 5 January 2023 doi:10.20944/preprints202301.0090.v1

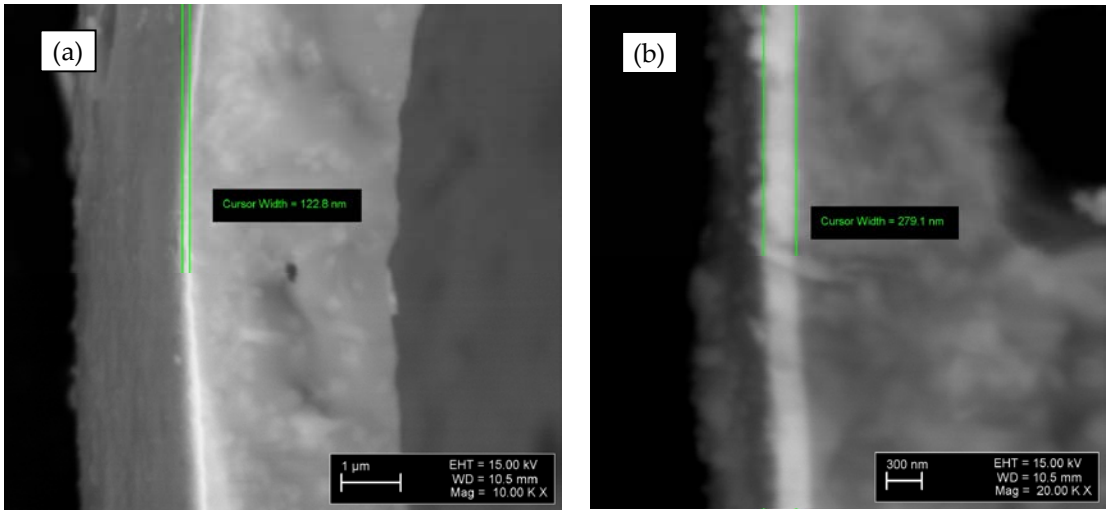

Figure 8. SEM micrographs of the Ti@CS (a) and Ti-TiN@CS (b)

Figure 8 shows the Ti-deposited layer (122.8 nm) on the CS2 (Figure 7a), and Ti-TiN deposited layers (279.1 nm) on the CS2 (Figure 7b). However, multiple measurements, noted that the layer thickness of Ti (for Ti@CS) is between 100 to 350 nm of thickness; and in the case of Ti-TiN@CS layer of TiN nitride is between 90 and 350 nm and Ti between 150 and 380 nm. The deposited Ti and Ti-TiN coatings in all observed specimens is intact and has no crack, pores or delamination.

3.5. *The behaviour of the CS at elevated temperature*

Using HTM, 2D-dilatometry curves were obtained that describe changes in the volume or linear dimensions of CS under the influence of temperature. As can be seen from the curves in **Figure 9**, the patterns made of CS1 and CS2 the deformation is negligible till

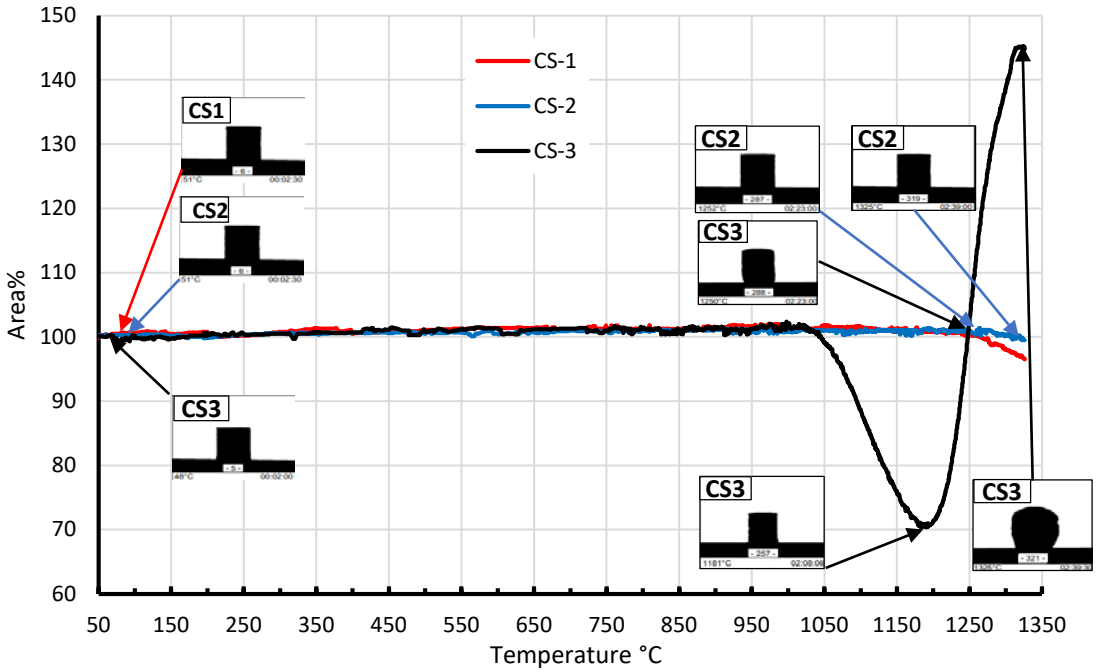

Figure 9. CS1, SC2 and CS3 2D-dilatometry curves in the 50-1325 °C temperatures interval.

 doi:10.20944/preprints202301.0090.v1

the 1200-1325 °C temperatures interval, but after this temperature, a slight shrinkage can be observed, which could be due to the deformation of the CS and their mutual compaction (softening begins). At a sample CS3 temperature above 1050 °C, a sharp shrinkage of the sample occurs, which is due to the transition of the sample into a semi-pyroplastic state, which could be caused by the presence of K_2O and Fe_2O_3, which lowers the softening point of the sample (T_g). Starting from 1190-1200 °C, a sharp increase in volume begins, which is associated with the release of gases.

As can be seen in **Figure 10**, heating to 1200 °C does not cause visually detectable changes for cenospheres CS1 and CS2 practically does not cause visually detectable changes, but a slight change in the colour of CS1 is observed, which can be explained by the burnout of coal particles and the oxidation of the Fe present in small quantities, which is black, to Fe_2O_3, which has a reddish-brown colour. In the case of sample CS3, a significant discolouration and compaction of the sample is observed already at 1100 °C, and even more pronounced at 1200 °C. Visually observed phenomena are consistent with the HTM experiment's data.

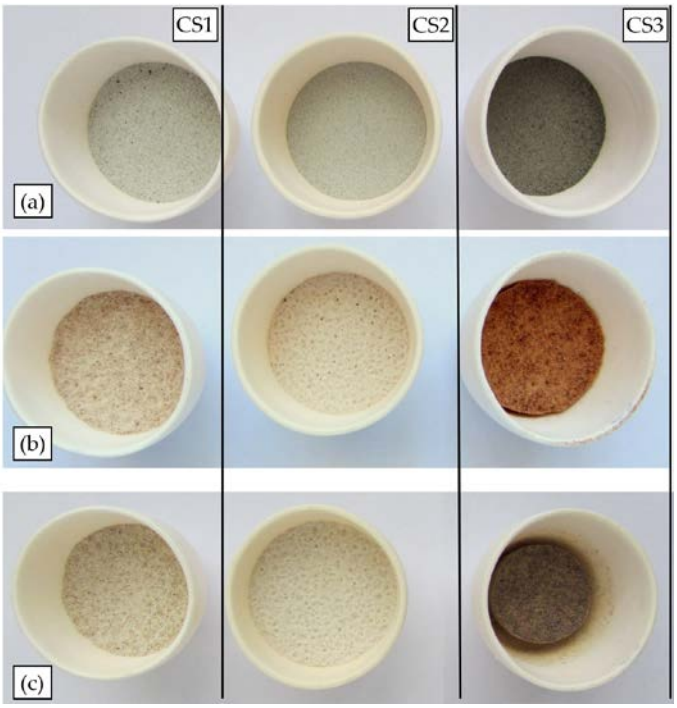

Figure 10. Images of censopheres at various stages of heat treatment (a) as received, (b) 1100 °C and (c) 1200 °C.

3.6. Specific thermal conductivity coefficient

Specific thermal conductivity is an important physical parameter in case of properties prediction of CS made composites. The thermal conductivities obtained from experiments are 0.109±0.0005, 0.100±0.0005, and 0.096±0.0005 $W \cdot m^{-1} \cdot K^{-1}$ for CS1, CS2, and CS3. The obtained data on the thermal conductivity of CS allows us to conclude that if these particles are used as filler in any matrix, a very low thermal conductivity can be achieved. This is primarily due to the fact that the particles are mostly air, and the wall is a highly insulating mixture of ceramics.

The indicators, which were determined during the research (chemical composition, thermal conductivity, bulk density) for samples CS1, CS2 are rather similar, but for CS3 they somewhat differ. Sample CS3 differs from CS1 and CS2 considerably with its thermal

 doi:10.20944/preprints202301.0090.v1

durability – these cenopheres sinter and shrink considerably. It can be due to the relatively greater number of particles with d<63 μm, and a higher content of volatile and combustible carbon, at around 3.9 % (mass). It was also observed that a greater amount of amorphous phase was present after heat treatment, with greater contents of SiO_2.

4. Conclusions

Physical and chemical properties of microballoons of aluminosilicates called cenospheres were studied, which are produced as a by-product (flyash) of burning coal. Several sources flyash from of coal basins in thermal power plants were selected. Cenospheres with particle sizes ranging from 40 to 500 μm were studied. Different particle distribution by size is observed, a more uniform distribution of CS particles is in the case of CS2: above 74% with dimensions from 100 to 150 μm. CS bulk has a similar density for all samples and amounts to around 0,4 $g \cdot cm^{-3}$, with a particle shell material density of 2.1 $g \cdot cm^{-3}$.

Energy dispersive X-ray spectrometry (EDS) and chemical analysis of the CS revealed that the main components of the studied CS are SiO_2 and Al_2O_3, in the case of CS1 and CS2, the sum of these components is on average from 93 to and 95%. In the case of CS3, the sum of SiO_2 and Al_2O_3 does not exceed 86 %, Fe_2O_3 and K_2O are present in quantities appreciable in CS3.

The presence of SiO_2 and Al_2O_3 in the composition of micro balloons is also confirmed by spectroscopic studies of FTIR. As shown by X-ray studies, the diffractograms of the samples CS1 and CS2 are very similar, in the output samples, one can mainly observe the mullite $Al_6Si_2O_{13}$ and the amorphous phase. In the output samples of CS3, the quartz and amorphous phases can be observed mainly, the heat treatment causes a decrease in the quartz phase, and the crystalline phase of mullite appears.

The thermal conductivity of samples of all CS varies from 0.096 to 0.109 $W \cdot m^{-1} \cdot K^{-1}$. The chemical composition, size distribution and structure of the cenosphere affect their thermal stability. Cenospheres types CS1, CS2, do not sinter during heat treatment up to 1200 °C, while the sample CS3 is subjected to sintering already at 1100 °C, making it a bad choice for SF development. This behaviour in CS3 is attributed to the softening of the structure due to the presence of Fe_2O_3 and K_2O.

Due to the properties discussed above, sample CS2 was selected for further experiments. Better thermal stability, narrow grading composition, and more uniform particle size distribution (94.2% of particles have size of 63-150 μm) (Table 3). Morphology is also unform with high sphericity and very low presence of agglomerates. Although there was a significantly higher percentage of defective particles in the as received CS, post-sieved product was of a high quality.

Author Contributions: Conceptualization, A.S. and J.O.; methodology, I.Z., G.M.; validation, V.P. and A.K.S.; formal analysis, A.S.; investigation, V.A., I.Z and A.S.; resources, A.S.; data curation, V.A., A.S.; writing—original draft preparation, A.S., J.O. G.M.; writing—review and editing, A.S. and A.K.S.; visualisation, V.A., I.Z. and V.P.; supervision, J.O and A.S.; project administration, A.S.; funding acquisition, A.S. All authors have read and agreed to the published version of the manuscript.

Funding: This research was funded by VPP AIPP project Nr. VPP-AIPP-2021/1-0015 "Combined lightweight, high-temperature resistant hybrid composite for combined protection of drones from Direct Energy Weapon". The article was published with the financial support from the Riga Technical University Research Support Fund.

Institutional Review Board Statement: Not applicable.

Informed Consent Statement: Not applicable.

Data Availability Statement: Not applicable.

Conflicts of Interest: The authors declare no conflict of interest.

References

1. Gupta, N.; Rohatgi, P.K. *Metal Matrix Syntactic Foams: Processing, Microstructure, Properties and Applications*; Gupta, N., Ed.; DEStech Publications, Inc: Lancaster, 2014; ISBN 978-1932078831.
2. John, B.; Nair, C. *Update on Syntactic Foams*; 2010; ISBN 9781847351203.
3. Thiyagarajan, R.; Senthil kumar, M. A Review on Closed Cell Metal Matrix Syntactic Foams: A Green Initiative towards Eco-Sustainability. *Materials and Manufacturing Processes* **2021**, *36*, 1333–1351, doi:10.1080/10426914.2021.1928696.
4. Yousaf, Z.; Morrison, N.F.; Parnell, W.J. Tensile Properties of All-Polymeric Syntactic Foam Composites: Experimental Characterization and Mathematical Modelling. *Compos B Eng* **2022**, *231*, 109556, doi:10.1016/J.COMPOSITESB.2021.109556.
5. Singh, A.K.; Saltonstall, B.; Patil, B.; Hoffmann, N.; Doddamani, M.; Gupta, N. Additive Manufacturing of Syntactic Foams: Part 2: Specimen Printing and Mechanical Property Characterization. *JOM* **2018**, *70*, 310–314, doi:10.1007/s11837-017-2731-x.
6. Gupta, N.; Zeltmann, S.E.; Shunmugasamy, V.C.; Pinisetty, D. Applications of Polymer Matrix Syntactic Foams. *JOM* **2014**, *66*, 245–254, doi:10.1007/S11837-013-0796-8.
7. Rohatgi, P.K.; Gupta, N.; Schultz, B.F.; Luong, D.D. The Synthesis, Compressive Properties, and Applications of Metal Matrix Syntactic Foams. *JOM* **2011**, *63*, 36–42, doi:10.1007/S11837-011-0026-1.
8. Ranjbar, N.; Kuenzel, C. Cenospheres: A Review. *Fuel* **2017**, *207*, 1–12, doi:10.1016/j.fuel.2017.06.059.
9. Adesina, A. Sustainable Application of Cenospheres in Cementitious Materials – Overview of Performance. *Developments in the Built Environment* **2020**, *4*, 100029, doi:10.1016/J.DIBE.2020.100029.
10. *Cenosphere Market - Global Forecast to 2022*; 2022;
11. Shao, Y.; Jia, D.; Liu, B. Characterization of Porous Silicon Nitride Ceramics by Pressureless Sintering Using Fly Ash Cenosphere as a Pore-Forming Agent. *J Eur Ceram Soc* **2009**, *29*, 1529–1534, doi:10.1016/j.jeurceramsoc.2008.09.012.
12. Rohatgi, P.K.; Matsunaga, T.; Gupta, N. Compressive and Ultrasonic Properties of Polyester/Fly Ash Composites. *J Mater Sci* **2009**, *44*, 1485–1493, doi:10.1007/s10853-008-3165-1.
13. Anshits, N.N.; Vereshchagina, T.A.; Bayukov, O.A.; Salanov, A.N.; Anshits, A.G. The Nature of Nanoparticles of Crystalline Phases in Cenospheres and Morphology of Their Shells. *Glass Physics and Chemistry* **2005**, *31*, 306–315, doi:10.1007/s10720-005-0060-6.
14. Bride, S.P.M.; Shukla, A. Processing and Characterization of a Lightweight Concrete Using Cenospheres. **2002**, *7*, 4217–4225.
15. Kulkarni, M.; Bambole, V.; Mahanwar, P. Effect of Particle Size of Fly Ash Cenospheres on the Properties of Acrylonitrile Butadiene Styrene-Filled Composites. *Journal of Thermoplastic Composite Materials* **2012**, *27*, 251–267, doi:10.1177/0892705712443253.
16. Chauhan, S.; Thakur, S. Effect of Micro Size Cenosphere Particles Reinforcement on Tribological Characteristics of Vinylester Composites under Dry Sliding Conditions. *Journal of Minerals and Materials Characterization and Engineering* 2012, *11*, 938.

17. Rohatgi, P.K.; Kim, J.K.; Gupta, N.; Alaraj, S.; Daoud, A. Compressive Characteristics of A356/Fly Ash Cenosphere Composites Synthesized by Pressure Infiltration Technique. *Compos Part A Appl Sci Manuf* **2006**, *37*, 430–437, doi:10.1016/j.compositesa.2005.05.047.
18. Dou, Z.Y.; Jiang, L.T.; Wu, G.H.; Zhang, Q.; Xiu, Z.Y.; Chen, G.Q. High Strain Rate Compression of Cenosphere-Pure Aluminum Syntactic Foams. *Scr Mater* **2007**, *57*, 945–948, doi:10.1016/j.scriptamat.2007.07.024.
19. Sankaranarayanan, S.; Nguyen, Q.B.; Shabadi, R.; Almajid, A.H.; Gupta, M. Powder Metallurgy Hollow Fly Ash Cenospheres' Particles Reinforced Magnesium Composites. *Powder Metallurgy* **2016**, *59*, 188–196, doi:10.1080/00325899.2016.1139339.
20. Wang, M.-R.; Jia, D.-C.; He, P.-G.; Zhou, Y. Microstructural and Mechanical Characterization of Fly Ash Cenosphere/Metakaolin-Based Geopolymeric Composites. *Ceram Int* **2011**, *37*, 1661–1666, doi:10.1016/j.ceramint.2011.02.010.
21. Shishkin, A.; Mironovs, V.; Zemchenkovs, V.; Hussainova, I. Metal Powder/Fly Ash Cenosphere/Modified Clay, Composite. In Proceedings of the Euro PM 2014 Congress and Exhibition, Proceedings; 2014.
22. Castellanos, A.G.; Mawson, H.; Burke, V.; Prabhakar, P. Fly-Ash Cenosphere/Clay Blended Composites for Impact Resistant Tiles. *Constr Build Mater* **2017**, *156*, 307–313, doi:10.1016/j.conbuildmat.2017.08.151.
23. Bharath Kumar, B.R.; Zeltmann, S.E.; Doddamani, M.; Gupta, N.; Uzma; Gurupadu, S.; Sailaja, R.R.N. Effect of Cenosphere Surface Treatment and Blending Method on the Tensile Properties of Thermoplastic Matrix Syntactic Foams. *J Appl Polym Sci* **2016**, *133*, doi:10.1002/app.43881.
24. Bharath Kumar, B.R.; Doddamani, M.; Zeltmann, S.E.; Gupta, N.; Uzma; Gurupadu, S.; Sailaja, R.R.N. Effect of Particle Surface Treatment and Blending Method on Flexural Properties of Injection-Molded Cenosphere/HDPE Syntactic Foams. *J Mater Sci* **2016**, *51*, 3793–3805, doi:10.1007/s10853-015-9697-2.
25. Irtiseva, K.; Lapkovskis, V.; Mironovs, V.; Ozolins, J.; Thakur, V.K.; Goel, G.; Baronins, J.; Shishkin, A. Towards Next-Generation Sustainable Composites Made of Recycled Rubber, Cenospheres, and Biobinder. *Polymers (Basel)* **2021**, *13*, 574, doi:10.3390/polym13040574.
26. Shishkin, A.; Hussainova, I.; Kozlov, V.; Lisnanskis, M.; Leroy, P.; Lehmhus, D. Metal-Coated Cenospheres Obtained via Magnetron Sputter Coating: A New Precursor for Syntactic Foams. *JOM* **2018**, *70*, 1319–1325, doi:10.1007/s11837-018-2886-0.
27. Shishkin, A.; Drozdova, M.; Kozlov, V.; Hussainova, I.; Lehmhus, D. Vibration-Assisted Sputter Coating of Cenospheres: A New Approach for Realizing Cu-Based Metal Matrix Syntactic Foams. *Metals (Basel)* **2017**, *7*, 16, doi:10.3390/met7010016.
28. Hales, T. A Proof of the Kepler Conjecture. *Ann Math* **2005**, *162*, 1065–1185, doi:10.4007/annals.2005.162.1065.
29. Hales, T.C. Historical Overview of the Kepler Conjecture. *Discrete Comput Geom* **2006**, *36*, 5–20, doi:10.1007/s00454-005-1210-2.
30. SCOTT, G.D. Packing of Spheres: Packing of Equal Spheres. *Nature* **1960**, *188*, 908–909, doi:10.1038/188908a0.
31. Scott, G.D.; Kilgour, D.M. The Density of Random Close Packing of Spheres. *J Phys D Appl Phys* **1969**, *2*, 311, doi:10.1088/0022-3727/2/6/311.
32. Shishkin, A.; Drozdova, M.; Kozlov, V.; Hussainova, I.; Lehmhus, D. Vibration-Assisted Sputter Coating of Cenospheres: A New Approach for Realizing Cu-Based Metal Matrix Syntactic Foams. *Metals (Basel)* **2017**, *7*, doi:10.3390/met7010016.

33. Reig, F.B.; Adelantado, J.V.G.; Moya Moreno, M.C.M. FTIR Quantitative Analysis of Calcium Carbonate (Calcite) and Silica (Quartz) Mixtures Using the Constant Ratio Method. Application to Geological Samples. *Talanta* **2002**, *58*, 811–821, doi:10.1016/S0039-9140(02)00372-7.